Ionospheric electron enhancement preceding
the 2011 Tohoku-Oki earthquake

Kosuke Heki

Dept. Natural History Sci., Hokkaido University
N10 W8, Kita-ku, Sapporo, Hokkaido 060-0810, Japan
Email: heki@mail.sci.hokudai.ac.jp

Abstract

The 2011 March 11 Tohoku-Oki earthquake (M_w9.0) caused vast damages to the country. Large events beneath dense observation networks could bring breakthroughs to seismology and geodynamics, and here I report one such finding. The Japanese dense network of Global Positioning System (GPS) detected clear precursory positive anomaly of ionospheric total electron content (TEC) around the focal region. It started ~40 minutes before the earthquake and reached nearly ten percent of the background TEC. It lasted until atmospheric waves arrived at the ionosphere. Similar preseismic TEC anomalies, with amplitudes dependent on magnitudes, were seen in the 2010 Chile earthquake (M_w8.8), and possibly in the 2004 Sumatra-Andaman (M_w9.2) and the 1994 Hokkaido-Toho-Oki (M_w8.3) earthquakes, but not in smaller earthquakes.

1. Introduction

Various kinds of earthquake precursors have been reported so far [*Rikitake*, 1976]. Among others, electromagnetic phenomena have been explored worldwide, e.g. electric currents in the ground [*Uyeda and Kamogawa*, 2008], propagation anomaly of VLF [*Molchanov and Hayakawa*, 1998] and VHF [*Moriya et al.*, 2010] radio waves. They are based on measurements by purpose-built instruments at discrete observing points. Hence it has been difficult to verify their spatial correlation with earthquakes. Spatial coverage could be improved by satellite observations [*Němec et al.*, 2008], but it is difficult to monitor the region of future earthquakes continuously.

The 2011 March 11 (05:46UT) Tohoku-Oki earthquake ruptured the plate boundary ~450 km in length and ~200 km in width along the Japan Trench where the Pacific Plate subducts beneath NE Japan (Fig.1). GEONET (GPS Earth Observation Network) is composed of >1000 continuous GPS stations. It has been yielding useful crustal deformation data since its launch

in 1994 [*Heki*, 2007], and already revealed coseismic and early postseismic crustal movements of the Tohoku-Oki earthquake [*Ozawa et al.*, 2011]. GEONET offers continuous measurements of nearly two-dimensional crustal movements of the country. Although it could detect mm level precursory crustal deformation of earthquakes, there have been no such reports to date. GPS can also measure TEC, ionospheric electron contents integrated along line-of-sights, by using the phase differences between the two L-band carrier waves. Here I focus on the two-dimensional TEC distribution above Japan and its behavior immediately before the 2011 Tohoku-Oki earthquake.

2. TEC Changes in the 2011 Tohoku Earthquake

A popular seismological target of GPS-TEC studies has been coseismic ionospheric disturbances (CID) caused by various atmospheric waves generated by earthquakes [*Calais and Minster*, 1995]. They include direct acoustic waves excited by vertical crustal movements [*Heki et al.*, 2006], Rayleigh surface waves [*Rolland et al.*, 2011a], and internal gravity waves [*Occhipinti et al.*, 2008]. Fig.1A shows the TEC behavior before and after the earthquake seen from a GPS station in NE Japan. At the time of earthquake (5:46UT), eight GPS satellites were visible there (Fig.1B). CIDs are clearly seen with satellites 5, 15, 26, 27, 28 as the irregular TEC changes caused by acoustic waves ~10 minutes after the earthquake, and with satellites 18 and 22 as the oscillatory variations caused by internal gravity waves 40-80 minutes after the earthquake [*Rolland et al.*, 2011b]. I try to isolate non-oscillatory TEC anomalies immediately before the earthquake, which are not readily visible in Fig.1A.

Fig. 2 shows slant TEC changes over ~5 hours period observed at five GPS stations with the satellite 15. The TEC shows gentle curvature due to satellite elevation changes. I employ the data analysis procedure used for the detection of ballistic missile signatures in TEC [*Ozeki and Heki,* 2010] (see Auxiliary Material). In addition to CID, transient positive anomaly of TEC is seen to start ~40 minutes before the earthquake. Fig. 2B shows trajectories of sub-ionospheric points (SIP) assuming a thin layer at 300 km altitude. The TEC anomaly is larger for the SIP closer to the epicenter, and reaches ~4 TECU (1 TECU is 10^{16} electrons/m^2). On the other hand, slight negative TEC anomaly is seen at GPS stations with SIP distant from the epicenter. These anomalies disappear and TEC returns to normal after CID arrivals.

Fig. 3 shows three snapshots of the geographical distribution of such TEC anomalies. There are little anomalies 1 hour before the earthquake (Fig.3A). Positive anomalies have already emerged in NE Japan 20 minutes before the earthquake (Fig.3B), and become larger toward the earthquake occurrence time (Fig.3C). Slight negative changes of TEC are also seen in SW Japan. The maximum positive anomaly of vertical TEC is ~2.3 TECU, which corresponds to ~8 % of the background value (~27 TECU according to the global ionospheric

map [*Mannucci et al.*, 1998] of this day). The latitudinal extent of the positive TEC anomaly approximately overlaps with the ruptured fault segments. Similar figures to Figs. 2 and 3 were drawn using three other satellites 27, 26, 9, and are shown in Figs. S1, 3, 5 and S2, 4, 6, respectively. The spatial extent and amplitudes of the positive anomalies seems to vary slightly from satellite to satellite. This would reflect the three-dimensional nature of the electron density change which is projected onto a thin layer at 300 km altitude in drawing these figures.

Global ionospheric maps (GIM) calculated from worldwide GPS stations have spatial resolution of 2.5/5 degrees in latitude/longitude [*Mannucci et al.*, 1998]. I downloaded the model (codg0700.11i) from University of Berne (ftp.unibe.ch), and added the slant TEC calculated for 0038/Sat.15 using this GIM to Fig.2A. Because the GPS station Mizusawa (mizu in Fig.2B), only ~200 km from the epicenter, is used in deriving the GIM, the synthesized curve also shows preseismic TEC enhancement although short wavelength components are lost due to its low spatial resolution.

3. Discussion

3.1. Past earthquakes

In order to find out if such TEC anomalies commonly precede earthquakes, I analyzed GPS data of the two recent M9 class earthquakes, the 2010 Central Chile (Maule) earthquake ($M_w8.8$) [*Moreno et al.*, 2010] and the $M_w9.2$ 2004 Sumatra-Andaman earthquake [*Banerjee et al.*, 2005]. Raw data files of Argentine continuous GPS stations on Feb. 27, 2010, have been downloaded from www.ign.gob.ar, and analyzed to see the TEC changes before the Chile earthquake. The TEC time series obtained with the satellite 17, sensitive to ionosphere close to the rupture area, show similar enhancement starting ~50 minutes before the earthquake and recovery after the CID arrival (Fig. 4 and Fig.S9). The anomaly is 3-4 TECU in slant TEC, somewhat smaller than the 2011 Tohoku earthquake.

CIDs of the 2004 Sumatra-Andaman earthquake have been analyzed using GPS stations in Indonesia and Thailand [*Heki et al.*, 2006]. SIP of the satellite 20 from Phuket (phkt) is very close to the epicenter, and the slant TEC time series there is found to show temporary increase exceeding 5 TECU lasting ~90 minutes (Figs.4 and S10). Although spatial coverage of GPS data in these two earthquakes is not sufficient, preseismic positive TEC anomaly appears to have accompanied these earthquakes.

In order to see if TEC enhancement occurs before smaller earthquakes, I analyzed GPS-TEC data of several largest earthquakes in time and region covered by GEONET. In the $M_w8.3$ 1994 Hokkaido-Toho-Oki earthquake [*Tsuji et al.*, 1995], the satellite 20 showed similar positive TEC anomaly starting ~60 minutes before the earthquake (Figs.4 and S11).

Although significant, the amount of anomaly is much smaller than those of the three M9 class earthquakes (Fig. 4). The 2003 Tokachi-Oki earthquake (M_w8.0) showed clear CID [*Heki and Ping*, 2005]. This earthquake, together with a few other M7-8 class earthquakes with clear CIDs, did not show significant preseismic TEC anomalies (Fig.S12). Fig.4B summarizes the magnitude dependence of the vertical TEC enhancement immediately before the earthquake.

3.2. Models

There are no conclusive models for the preseismic electron enhancement. Here I give a few clues for future searches of the model. The smaller anomalies for the satellites 9/27 than 15/26 (auxiliary material) would be explained if ionospheric F-layer electrons are assumed to have moved down along the geomagnetic field. For example, we would see the positive TEC anomaly similar to the observation if electrons within a layer of 20 km thickness at 350 km height moved down to 300 km.

Electromagnetic earthquake precursors have been often attributed to positively charged aerosols [*Tributsch*, 1978]. Several hypotheses have been proposed for their sources. For example, experiments demonstrated that stresses mobilize positive holes in igneous rocks [*Takeuchi et al.,* 2006]. Alpha decay of radon released from the crust can also ionize the atmosphere. They may change the electric resistivity of the lower atmosphere, which could disturb the global electric circuit and redistribute ionospheric electrons [*Pulinets and Ouzounov*, 2011]

The disappearance of the enhanced TEC after the passage of CID would be understood as the mixing of ionosphere by acoustic waves. The amplitude of acoustic waves grows in the light upper atmosphere, e.g. a few parts of 0.1 mm/s vertical velocity at the ground level is amplified to >100 m/s at the F layer height [*Rolland et al.*, 2011a]. Such high-speed oscillations with periods of ~4.5 minute (atmospheric fundamental mode) would effectively homogenize the electron density irregularities formed before earthquakes.

One may consider that the TEC decrease associated with CID caused apparent preseismic TEC enhancement as an artifact. I demonstrate this is not the case in Figs. 4 and S3. I extrapolated the TEC model fitted for the period before 5.2 UT (i.e. before the precursor appeared) to the later period (gray dashed curves in Fig.4, and red curves in Fig.S3). The observed TEC keeps deviating positively from the extrapolated curves during the ~40 minutes period before the earthquake and CID brings them back to normal (i.e. it canceled out the anomalous preseismic enhancement by stirring the F layer). This is also confirmed by comparing the short-term TEC changing rates ~30 minutes before the earthquake between regions near the epicenter and those farther away (Fig. S7). Fig. S5 also shows an example of preseismic TEC enhancement without coseismic decrease.

4. Conclusions

Here I present an objectively testable scientific hypothesis that M9 class earthquakes are immediately preceded by positive TEC anomalies of magnitude-dependent amplitude lasting for an hour or so. Because the raw data files are available on the web, one can reproduce the results reported here. It is also easy to apply the method to other earthquakes. The possible precursor reported here is different qualitatively from past examples in three points, (1) obvious temporal correlation (immediately before earthquakes), (2) obvious spatial correlation (occurring around the focal area), and (3) clear magnitude dependence (Fig. 4B). The claim that earthquakes are inherently unpredictable [e.g. *Geller et al.,* 1997] might not be true at least for M9 class earthquakes.

A few points need to be cleared before the preseismic TEC enhancement can be used for short-term prediction of a large earthquake. A vital question is how often similar local TEC enhancement of non-earthquake origins occur. In Fig. S8, I compare the five hours slant TEC time series of the satellite 15 observed at 3009 from Jan.1 to Apr.30, 2011. They were all modeled with degree-3 polynomials. The precursory anomaly of the Tohoku-Oki earthquake was the largest of all. The second and the third largest anomalies (days 061 and 094) were found to have traveled southward suggesting their space weather origin (Fig.S8E,F). In order to discriminate such disturbances and preseismic TEC enhancements in real time, we may need to monitor TEC outside the Japanese Islands.

A rather technical issue is the separation of the real TEC changes from apparent changes due to satellite movements in the sky. At the moment, we need an arc of 1-2 hours or more to accurately separate satellite-specific biases from temporal changes of TEC. The situation will be improved by including Quasi-Zenith Satellite System (see qzss.jaxa.jp for detail). They are supposed to stay near zenith and will enable real time observations of vertical TEC changes.

References

Banerjee, P., F. F. Pollitz, and R. Bürgmann (2005), The size and duration of the Sumatra-Andaman earthquake from far-field static offsets, *Science, 308*, 1769-1772.

Calais, E., and. J. B. Minster (1995), GPS detection of ionospheric perturbations following the January17, 1994, Northridge earthquake, *Geophys. Res. Lett., 22*, 1045-1048, doi:10.1029/95GL00168.

Geller, R.J., D.D. Jackson, Y.Y. Kagan, and F. Mulargia (1997), Earthquakes cannot be predicted, *Science, 275*, 1616-1617,.

Heki, K. (2007), Secular, transient and seasonal crustal movements in Japan from a dense GPS array: Implication for plate dynamics in convergent boundaries, in *The Seismogenic Zone of Subduction Thrust Faults* edited by T. Dixon and C. Moore, pp. 512-539, Columbia University Press.

Heki, K. and J.-S. Ping (2005), Directivity and apparent velocity of the coseismic ionospheric disturbances observed with a dense GPS array, *Earth Planet. Sci. Lett., 236*, 845-855.

Heki, K., Y. Otsuka, N. Choosakul, N. Hemmakorn, T. Komolmis, and T. Maruyama (2006), Detection of ruptures of Andaman fault segments in the 2004 Great Sumatra Earthquake with coseismic ionospheric disturbances, *J. Geophys. Res., 111*, B09313, doi:10.1029/2005JB004202.

Mannucci, A.J., B.D. Wilson, D.N. Yuan, C.H. Ho, U.J. Lindqwister, and T.F. Runge (1998), *Radio Sci., 33*, 565-582.

Molchanov, O.A. and M. Hayakawa (1998), VLF signal perturbations possibly related to earthquakes, *J. Geophys. Res., 103*, 17489-17504.

Moreno, M., M. Bosenau, and O. Oncken (2010), 2010 Maule earthquake slip correlates with pre-seismic locking of Andean subduction zone, *Nature, 467*, 198-202.

Moriya, T., T. Mogi, and M. Takada (2010), Anomalous pre-seismic transmission of VHF-band radio waves resulting from large earthquakes, and its statistical relationship to magnitude of impending earthquakes, *Geophys. J. Int., 180*, 858-870.

Němec, F., O. Santolík, M. Parrot, and J. J. Berthelier (2008), Spacecraft observations of electromagnetic perturbations connected with seismic activity, *Geophys. Res. Lett., 35,* L05109, doi:10.1029/2007GL032517.

Occhipinti, G., E. A. Kherani, and P. Lognonné (2008), Geomagnetic dependence of ionospheric disturbances induced by tsunamigenic internal gravity waves, *Geophys. J. Int., 173*, 753-765.

Ozawa, S., T. Nishimura, H. Suito, T. Kobayashi, M. Tobita, and T. Imakiire (2011), Coseismic and postseismic slip of the 2011 magnitude-9 Tohoku-Oki earthquake, *Nature, 474*, doi:10.1038/nature10227.

Ozeki, M. and K. Heki (2010), Ionospheric holes made by ballistic missiles from North Korea detected with a Japanese dense GPS array, *J. Geophys. Res., 115*, A09314, doi:10.1029/2010JA015531.

Pulinets, S. and D. Ouzounov (2011), Lithosphere-atmosphere-ionosphere coupling (LAIC) model – A unified concept for earthquake precursor validation, *J. Asian Earth Sci.* 41, 371-382, doi:10.1016/j.jseaes.2010.03.005.

Rikitake, T. (1976), *Earthquake Prediction,* Elsevier, Amsterdam.

Rolland, L. M., P. Lognonné, and H. Munekane (2011a), Detection and modeling of Rayleigh wave induced patterns in ionosphere, *J. Geophys. Res., 116*, A05320, doi:10.1029/2010JA016161.

Rolland, L. M., P. Lognonné, E. Astafyeva, E.A. Kherani, N. Kobayashi, M. Mann, and H. Munekane (2011b), The resonant response of the ionosphere imaged after the 2011 off the Pacific coast of Tohoku Earthquake, *Earth Planets Space, 63*, in press.

Takeuchi, A., B.W.S. Lau, and F. Freund (2006), Current and surface potential induced by stress-activated positive holes in igneous rocks, *Phys. Chem. Earth., 31*, 240-247.

Tributsch, H. (1978), Do aerosol anomalies precede earthquakes? *Nature, 276*, 606-608.

Tsuji, H., Y. Hatanaka, T. Sagiya, and M. Hashimoto (1995), Coseismic crustal deformation from the 1994 Hokkaido-Toho-Oki earthquake monitored by a nationwide continuous GPS array in Japan, *Geophys.Res. Lett., 22*, 1669-1672.

Uyeda, S., M. Kamogawa (2008), The prediction of two large earthquakes in Greece, *EOS. Trans. Am. Geophys. Union, 89*, 363.

Figure Captions

Figure 1. (**A**) Time series 3.5-8.5 UT of slant TEC changes observed at 0035 (black square in **B**) with ten GPS satellites. Because each satellite-receiver pair has a different measurement bias, only their temporal changes are meaningful. CIDs are seen in almost all satellites after the main shock at 5:46. (**B**) Trajectories of SIP for the satellites shown in (**A**). On the trajectories, small red stars are SIP at 5:46 and small dots are hourly time marks. The rectangle shows the approximate rupture zone of this earthquake. The large red star shows the epicenter.

Figure 2. (**A**) Slant TEC change time series taken at five GPS stations with the satellite 15. Temporary positive TEC anomalies started ~40 minutes before the earthquake and disappeared after CID passages. Black smooth curves are the models (see Auxiliary Material), and anomalies are defined as the departure from the model curves. Slant TEC changes calculated using GIM for site 0038 is shown as the blue curve. (**B**) Positions of the fives GPS stations (red dots) and their 5:00-6:00UT SIP trajectories (blue dots indicate 5:46). The northernmost point is 0038. Then follow 0214, 3009, 0756 and 0596 southward.

Figure 3. Vertical TEC anomalies at three time epochs, (**A**) 1 hour, (**B**) 20 minutes, and (**C**) 1 minute before the earthquake, observed at GEONET stations with the satellite 15. Positive anomalies (red color) are seen to grow near the focal region.

Figure 4. (**A**) Slant TEC changes and their models in the 2011 Tohoku earthquake, the 2004 Sumatra-Andaman earthquake, the 1994 Hokkaido-Toho-Oki earthquake, and the 2010 Chile (Maule) earthquake. The horizontal axis shows the time from earthquakes. Dashed curves in gray for the top two time series show the models derived with data prior to the possible onset of the precursor (before 5.2 UT) and extrapolated to 5.2-6.0 UT. (**B**) Vertical TEC anomalies immediately before the earthquakes as a function of their moment magnitudes. Colors correspond to those in (**A**). In addition to the five data from four earthquakes in (**A**), three smaller earthquakes (Fig. S12) are included (white circles).
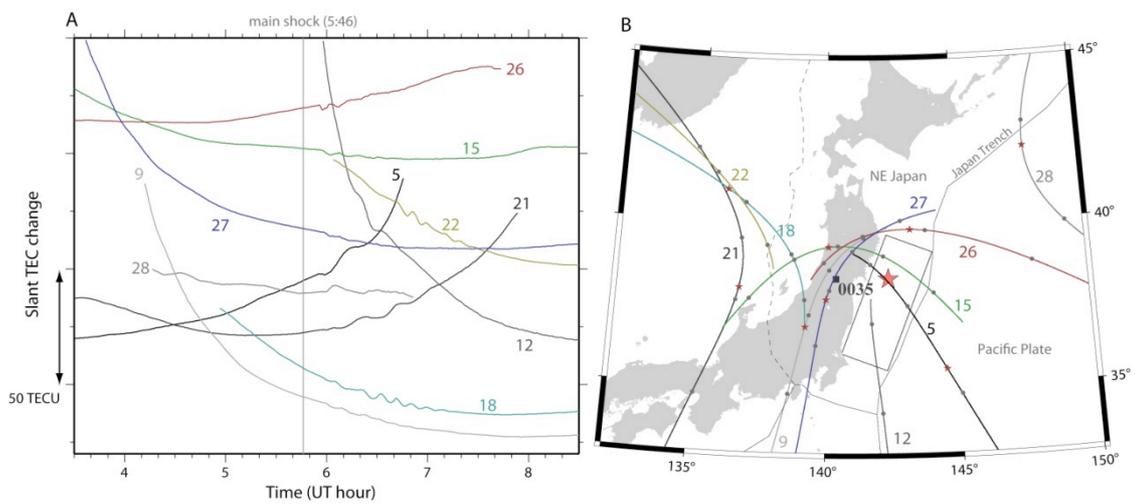
Figure 1
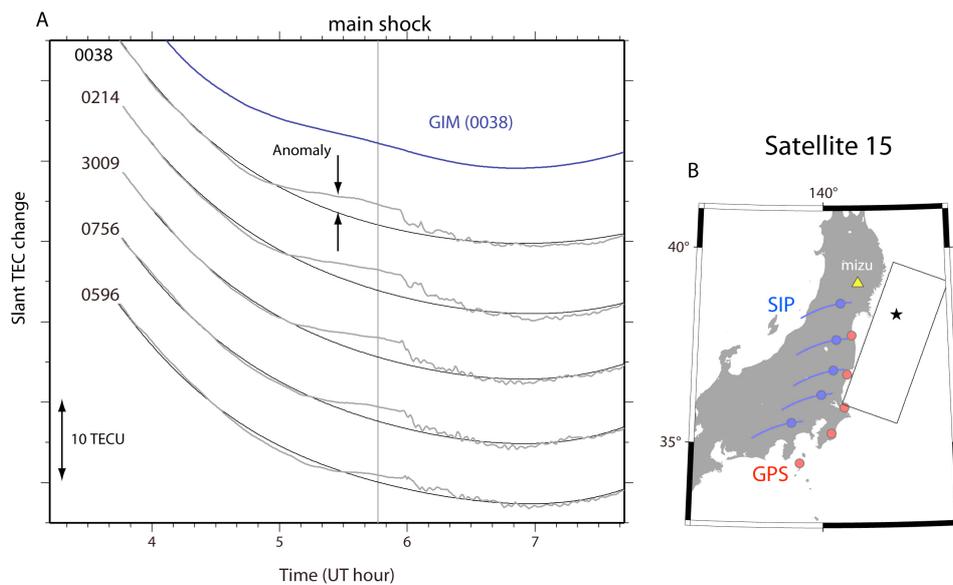
Figure 2
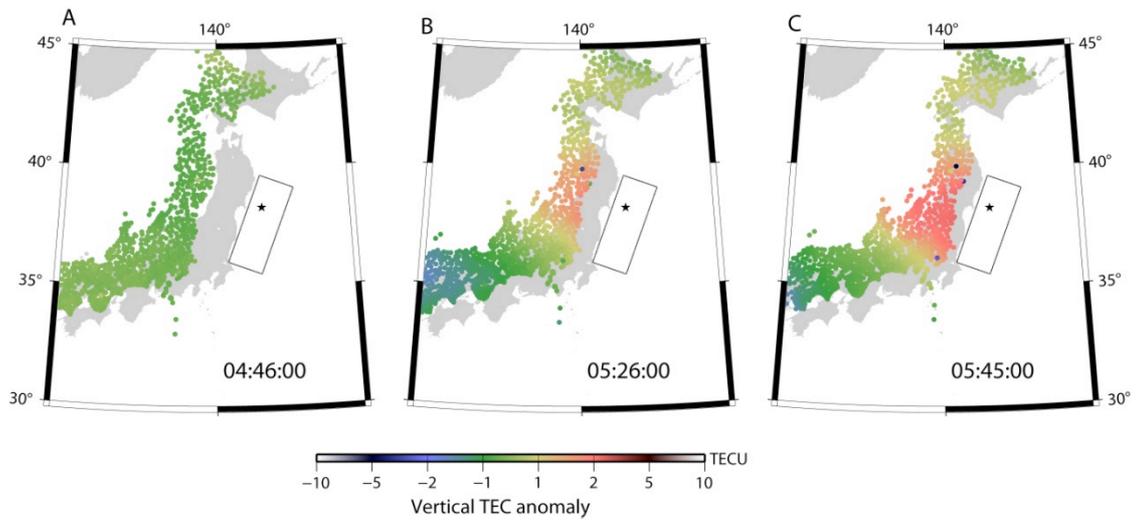
Figure 3
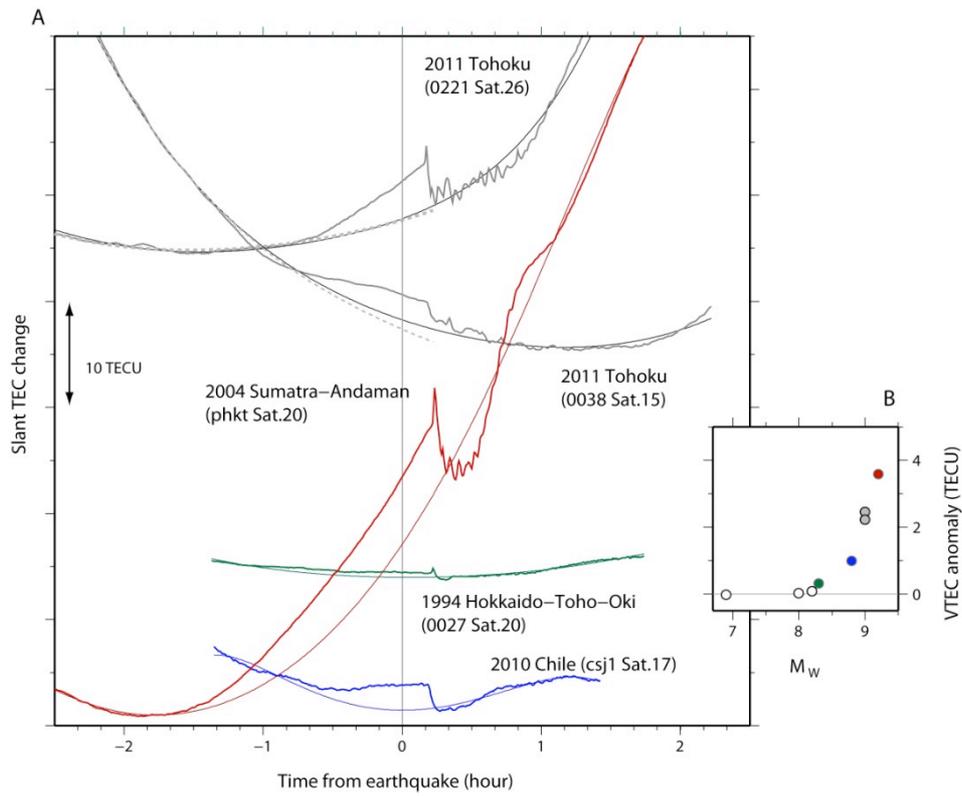
Figure 4

Auxiliary Material

Text S1

Method:

A GPS station records L-band carrier phases in two frequencies, 1.5 (L1) and 1.2 (L2) GHz, every 30 seconds (in GEONET). We downloaded the raw data on the day of the earthquake from terras.gsi.go.jp. Temporal changes of the differences between the two phases expressed in lengths are proportional to changes in TEC. To isolate the anomalous change of TEC, we model the raw TEC as a function of time t and angle ζ between line-of-sight and the local zenith at its ionospheric penetration point with a model,

$$\text{Slant TEC}(t, \zeta) = \text{VTEC}(t)/\cos\zeta + e, \tag{1}$$

where VTEC is the TEC when line-of-sight is perpendicular to the ionosphere. The bias e inherent to phase observables of GPS remains constant for individual satellites in the studied period. VTEC can be separated from e with a few hours of observations because ζ varies with time as the satellite moves in the sky (ζ can be calculated from orbital elements of GPS satellites). VTEC changes diurnally and its change in a few hours period can be well approximated with a cubic function of time t,

$$\text{VTEC}(t) = at^3 + bt^2 + ct + d. \tag{2}$$

I estimated a,b,c,d and e using the least-squares method using the time series 3:00-8:00 UT. In doing so, the period 5.2-6.0 UT, influenced by the preseismic TEC anomaly, was excluded (similar exclusion was done for other earthquakes in Fig.4 and S12). The estimated models are shown in Fig.2 with black smooth curves. The TEC anomaly was derived as the difference between the model and the observed TEC, and converted to vertical TEC anomaly (Fig.3) by multiplying with $\cos\zeta$.

Other satellites:

TEC changes in the 2011 Tohoku earthquake are plotted using the satellites 27 (Fig. S1), 26 (Fig. S3) and 9 (Fig. S5) in a similar manner to Fig. 2. The geographical distributions of TEC anomalies at three time epochs are given in Fig. S2 (satellite 27), S4 (satellite 26), and S6 (satellite 9). It is interesting that the satellites 27 and 9 (Fig. S2, S6) show smaller TEC anomalies than the satellites 15 (Fig.3) and 26 (Fig. S4). The angle between the line-of-sight and the geomagnetic field is smaller for the satellites 27 and 9 (< 30 degrees) than the other two satellites (50-70 degrees). Because ionospheric electron displacements in F layer are largely constrained along the geomagnetic field, increased and decreased parts might have

cancelled each other considerably in integrating the electron content along the line-of-sight for the satellites 27 and 9.

I demonstrate that the positive anomalies are not artifacts coming from coseismic TEC decrease in three different ways. First, model curves inferred using the time series before 5.2 UT were extrapolated assuming linear changes of VTEC to later hours (Fig. S3). They indicate that coseismic TEC decreases bring back the enhanced TEC to the state before the anomaly. Secondly, five minutes average changing rates of vertical TEC a half hour before the earthquake are mapped in Fig. S7. They show positive anomalies in NE Japan similar to Fig.3C although they are not influenced by coseismic TEC decreases. Thirdly, the northernmost station in Fig.S5 shows little coseismic TEC decrease (because its SIP at 05:45 UT is already away from the fault) although it shows clear preseismic positive anomaly.

Longer time window:

According to the space weather report (swc.nict.go.jp), geomagnetic activity on March 11 was relatively high due to the preceding corona hole activity. High geomagnetic activities often give rise to wavy TEC disturbances generated in the auroral belt and traveling southward (Large-scale traveling ionospheric disturbance, LSTID). However, local TEC enhancement stationary above a certain area, like the preseismic TEC anomaly shown in Fig.3, cannot be explained by such disturbances. It is also reported that strong sporadic E layer with the critical frequency exceeding 8 MHz did not appear in Japan on that day.

Fig. 8A-D shows the five hours time series of slant TEC observed at 3009 (blue square in Fig.8G) with the satellite 15 over the 4 months period in 2011. They were modeled using the degree-3 polynomial without excluding any parts of the time series. The maximum deviation from the model curve occurred on the day of the earthquake (red curve in Fig.8C, which is identical to the middle curve in Fig.2). The second and the third largest deviations (days 094 and 061) are considered to be LSTID propagating southward across the whole Japanese Islands. Fig. 8E, F shows their slant TEC time series at four GPS stations (red circles in Fig.8G), and their propagation is recognized by time shifts of the positive anomaly peaks.

Other earthquakes:

TEC time series in the 2010 Chile (Maule) earthquake and the 2004 Sumatra-Andaman earthquake are given in Figs. S9 and S10, respectively. In Fig.S10, the SIP of samp is closer to the epicenter than phkt. However, the SIP of phkt is closer to the fault segment with the largest moment release [*Banerjee et al.*, 2005]. This would be the reason why phkt showed larger

preseismic TEC anomaly than samp. Fig.S11 shows the TEC time series in the 1994 Hokkaido-Toho-Oki earthquake observed with the satellite 20 at five GPS stations. The CID of a few more earthquakes were observed with GEONET. They include the 2006 November Kuril earthquake ($M_w8.2$) [*Astafyeva and Heki*, 2009], the 2003 Tokachi-Oki earthquake ($M_w8.0$) and the foreshock of the 2004 September Off-Kii-Peninsula earthquake ($M_w6.9$) [*Heki and Ping*, 2005]. As seen in Fig. S12, they show only small (1994 Hokkaido-Toho-Oki and 2006 Kuril) or no (2003 Tokachi-Oki and 2004 Kii foreshock) preseismic TEC anomalies.

Auxiliary References:

Banerjee, P., F. F. Pollitz, and R. Bürgmann (2005), The size and duration of the Sumatra-Andaman earthquake from far-field static offsets, *Science, 308*, 1769-1772.

Astafyeva, E. and K. Heki (2009), Dependence of waveform of near-field coseismic ionospheric disturbance on focal mechanisms, *Earth Planets Space*, *61*, 939-943.

Heki, K. and J.-S. Ping (2005), Directivity and apparent velocity of the coseismic ionospheric disturbances observed with a dense GPS array, *Earth Planet. Sci. Lett., 236*, 845-855.

Heki, K. and K. Matsuo (2010), Coseismic gravity changes of the 2010 earthquake in Central Chile from satellite gravimetry, *Geophys. Res. Lett., 37*, L24306, doi:10.1029/2010GL045335.

Tsuji, H., Y. Hatanaka, T. Sagiya, and M. Hashimoto (1995), Coseismic crustal deformation from the 1994 Hokkaido-Toho-Oki earthquake monitored by a nationwide continuous GPS array in Japan, *Geophys.Res. Lett., 22*, 1669-1672.
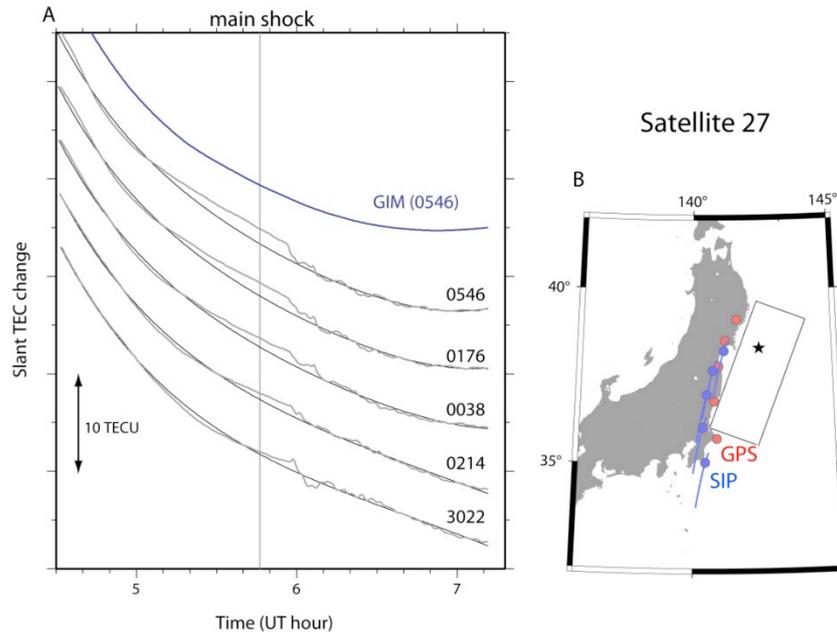
Figure S1. (**A**) Slant TEC change time series observed at five GPS stations with the satellite 27 showing preseismic TEC enhancement similar to the satellite 15 (Fig.2). Black smooth curves are the models derived assuming vertical TEC changing as cubic polynomials of time (the time window used for the fit is 4.0-7.2 UT). The blue curve shows the slant TEC changes calculated using GIM for site 0546. (**B**) Positions of the five GPS stations (red dots) in (**A**) and their 5:00-6:00 SIP trajectories (blue dots show 5:46).
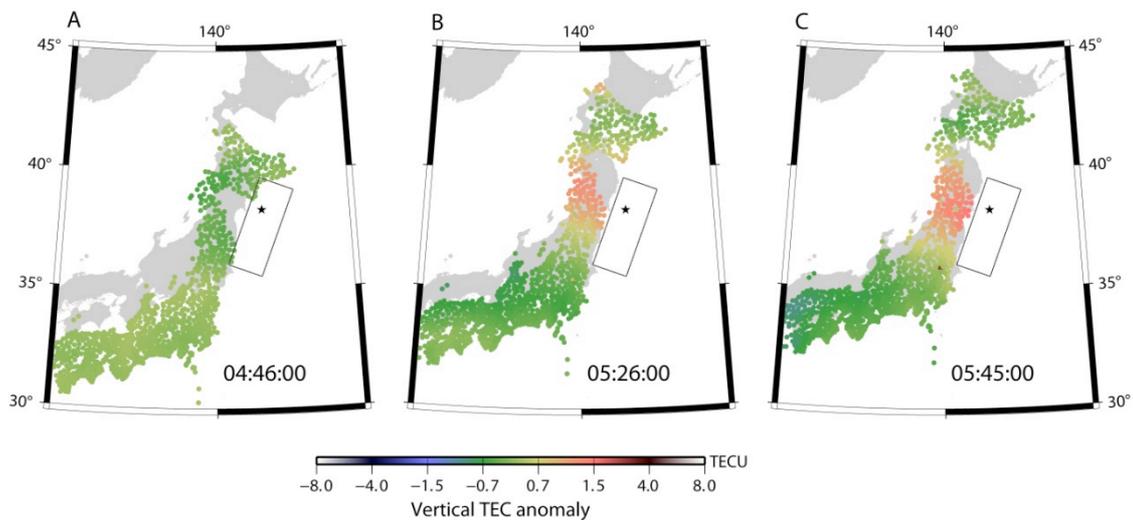
Figure S2. Snapshots of vertical TEC anomalies at (**A**) 1 hour, (**B**) 20 minutes, and (**C**) 1 minute before the earthquake observed with the satellite 27. Positive anomalies (red) are seen in the region similar to Fig. 3. Note that the anomalies are somewhat smaller than the satellites 15 (Fig.3) and 26 (Fig. S4).
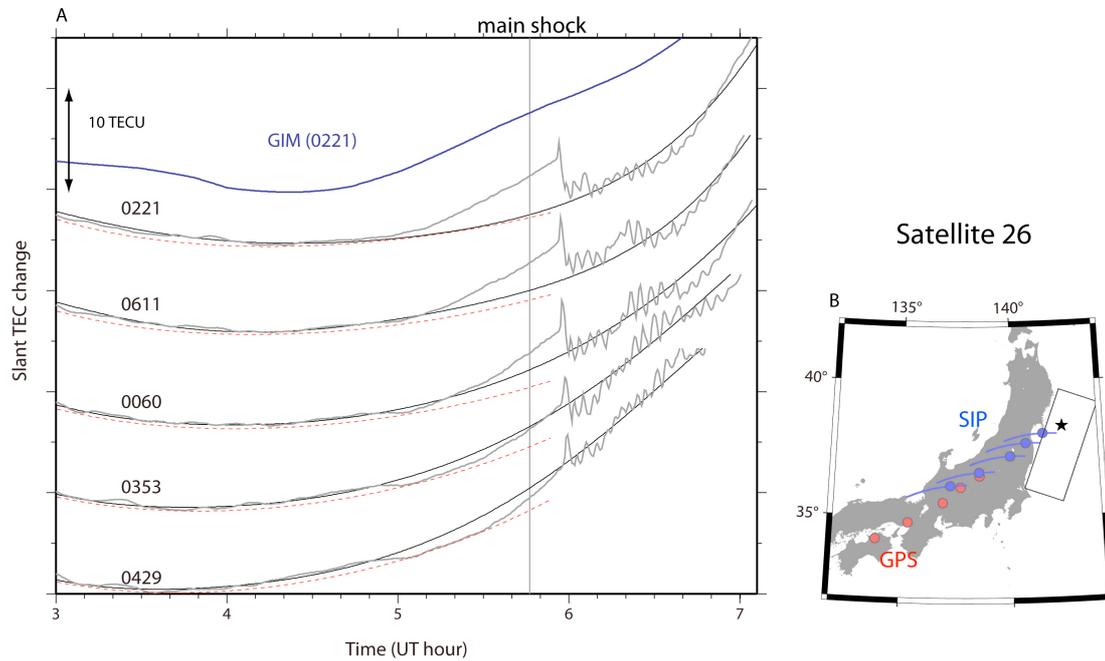
Figure S3. (**A**) Slant TEC change time series observed at five GPS stations with the satellite 26. Black smooth curves are the models derived assuming vertical TEC changing as cubic polynomials of time (the time window used for the fit is 2.5-8.0 UT). The blue curve shows the slant TEC changes calculated using GIM for site 0221. Dashed curves in red show the models (polynomial degree 1) derived with data prior to the precursor onset (5.2 UT) and extrapolated to the later period. (**B**) Positions of the five GPS stations (red dots) in (**A**) and their 5:00-6:00 SIP trajectories (blue dots show 5:46).
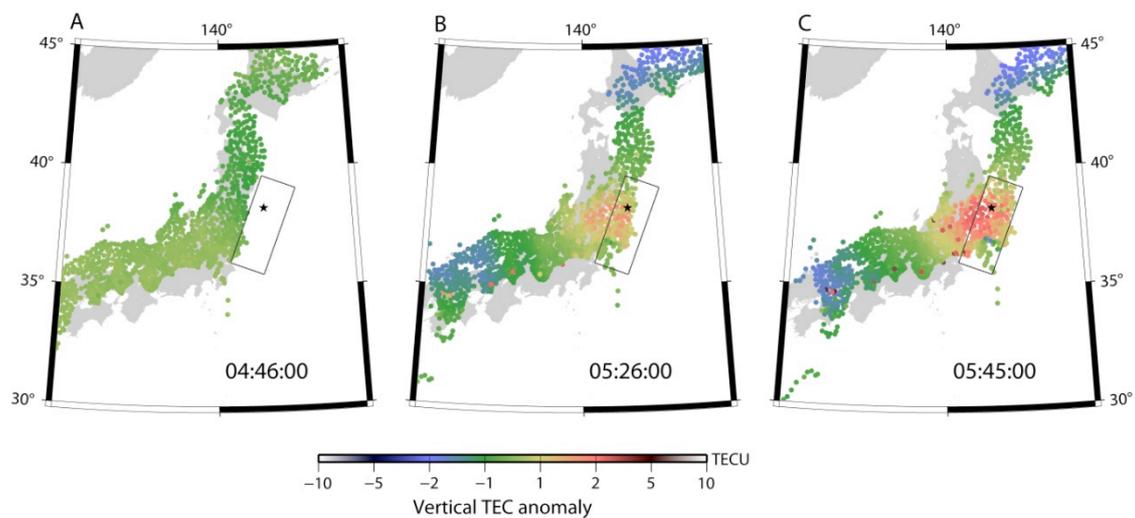
Figure S4. Vertical TEC anomalies at (**A**) 1 hour, (**B**) 20 minutes, and (**C**) 1 minute before the earthquake observed with the satellite 26. Positive anomalies (red) are seen to extend partly to the ocean.
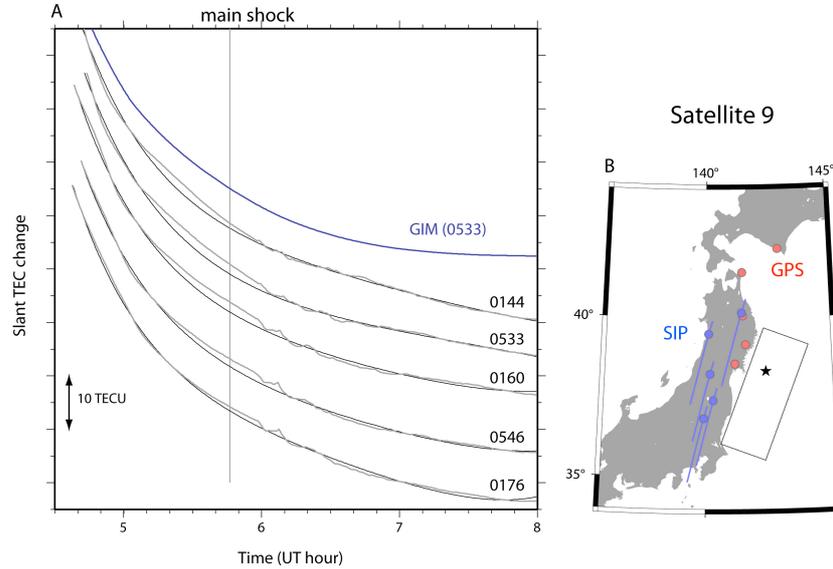
Figure S5. (**A**) Slant TEC change time series observed at five GPS stations with the satellite 9. Black smooth curves are the models derived assuming vertical TEC changing as cubic polynomials of time (the time window used for the fit is 4.3-8.0 UT). The blue curve shows the slant TEC changes calculated using GIM for site 0533. (**B**) Positions of the five GPS stations (red dots) in (**A**) and their 5:00-6:00 SIP trajectories (blue dots show 5:46). The station 0144 shows preseismic TEC enhancement but no coseismic decrease, suggesting that the former is not an artifact caused by the latter.
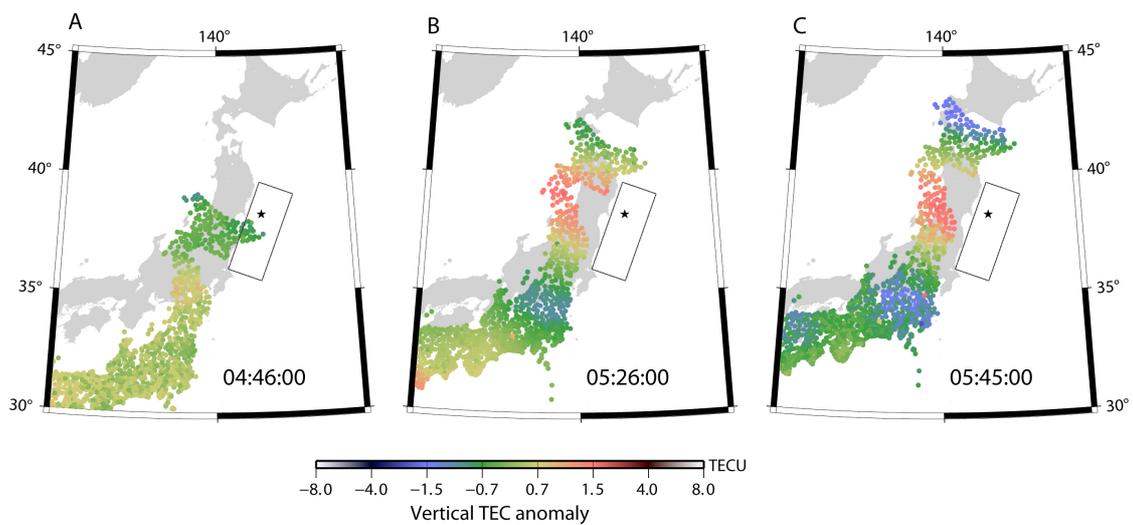
Figure S6. Vertical TEC anomalies at (**A**) 1 hour, (**B**) 20 minutes, and (**C**) 1 minute before the earthquake observed with the satellite 9. Note that the anomalies are smaller than the satellites 15 (Fig.3) and 26 (Fig. S4), and is similar to the satellite 27 (Fig. S2).
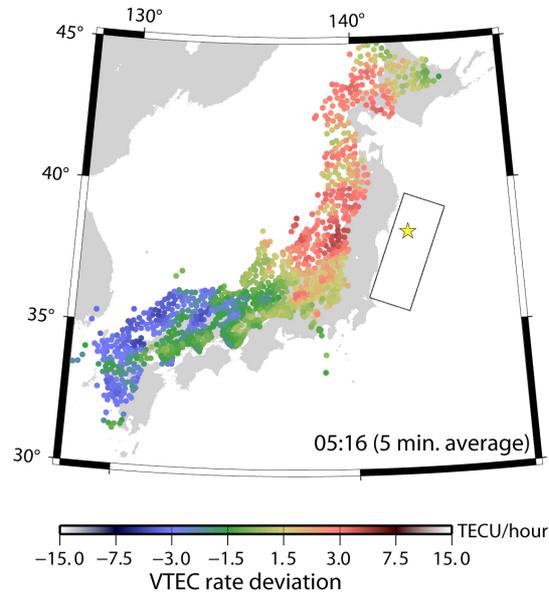
Figure S7. Average changing rate of vertical TEC over a five-minute period around 15:16 (30 minutes before the earthquake) of satellite 15 (derived from the time derivatives of slant TEC curves in Fig. 2). Color shows the deviation of the rate from the average of all the stations. It is seen that positive deviations are seen close to the rupture area.
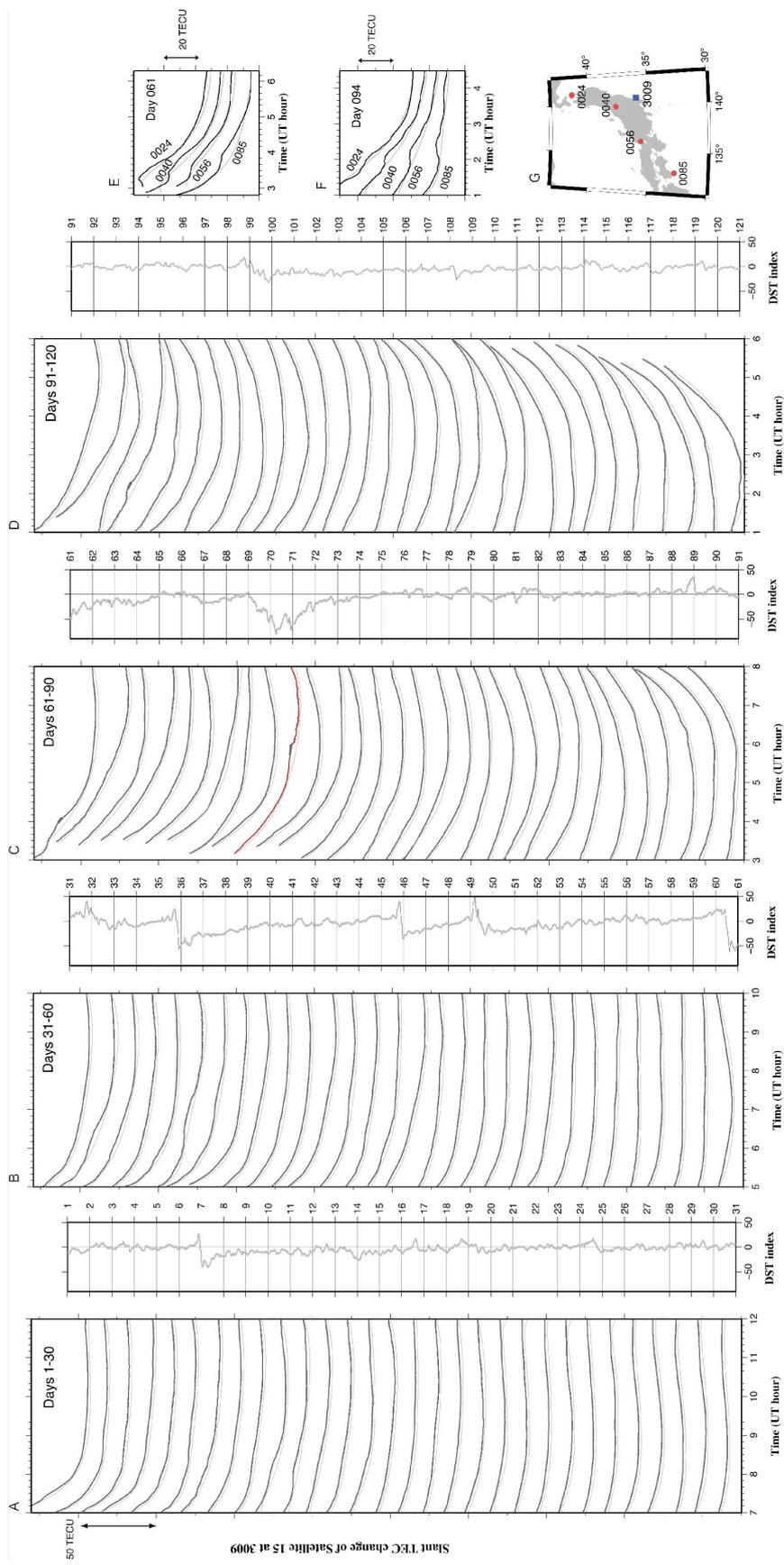
Figure S8. Slant TEC time series (thick curves) over five hours period observed at 3009 (blue square in **G**) with the satellite 15. **A** to **D** approximately correspond to January to April. Dst (disturbance space-time) indices (average disturbance of the north component of geomagnetic fields) are shown on the right-hand side. The time window is moved backwards two hours per month because the GPS orbital period is a half sidereal day (i.e. appearance of the satellite 15 becomes earlier by ~4 minutes per day). Thinner curves show models where VTEC are approximated with cubic functions of time (whole five hours periods shown in the figure are used). A small arbitrary negative offset is given in plotting the model curves to avoid overlap with the data. The root-mean-squares between the two curves were 0.34, 0.37, 0.56, 0.52 TECU for **A**, **B**, **C**, and **D**, respectively. The difference between the two curves exceeded 2.0 TECU (in VTEC) only once when preseismic TEC enhancement appeared (middle of the red curve in **C**). The difference exceeded 1.5 TECU in two more occasions around 4 UT on the day 061 and around 2 UT on the day 094 (marked with small black squares). They traveled southward as recognized by comparing TEC time series at four points (red circles in **G**) in **E** and **F**, respectively.
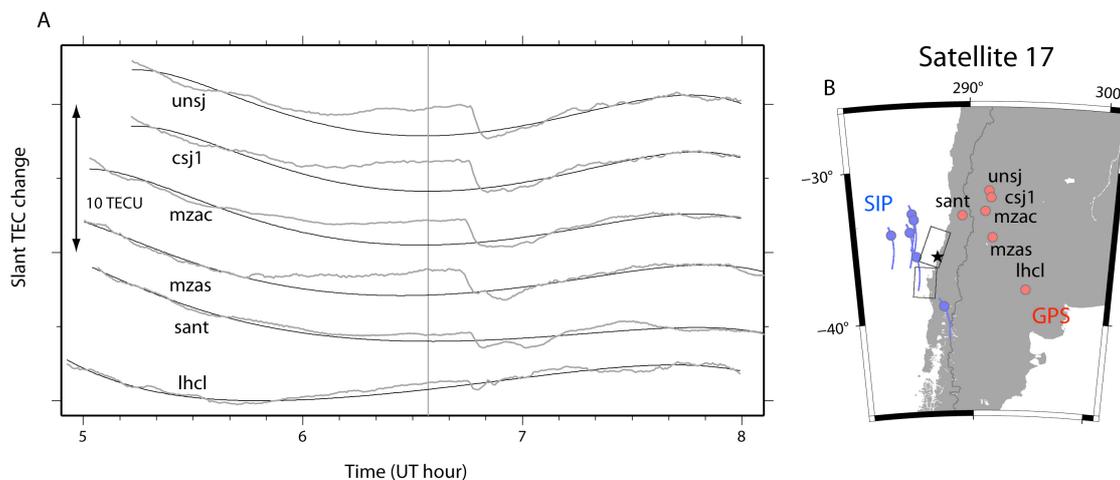
Figure S9. (**A**) Slant TEC change time series observed at six GPS stations in Chile/Argentine with the satellite 17. Black smooth curves are the models derived assuming vertical TEC changes as cubic polynomials of time (5.9-6.8 is excluded in estimating the model curves). The 2010 February 27 Maule earthquake occurred at 6:34 UT. Its fault planes [*Heki and Matsuo*, 2010] are shown by two rectangles in (**B**). Their 5.8-6.8 SIP trajectories (blue dots indicate 6:34) are plotted as blue curves. Preseismic electron enhancement seems to have started ~50 minutes before the earthquake as seen in the GPS stations, unsj, csj1, mzac, and mzas. The TEC increase is smaller at sant and is not clear in lhcl.
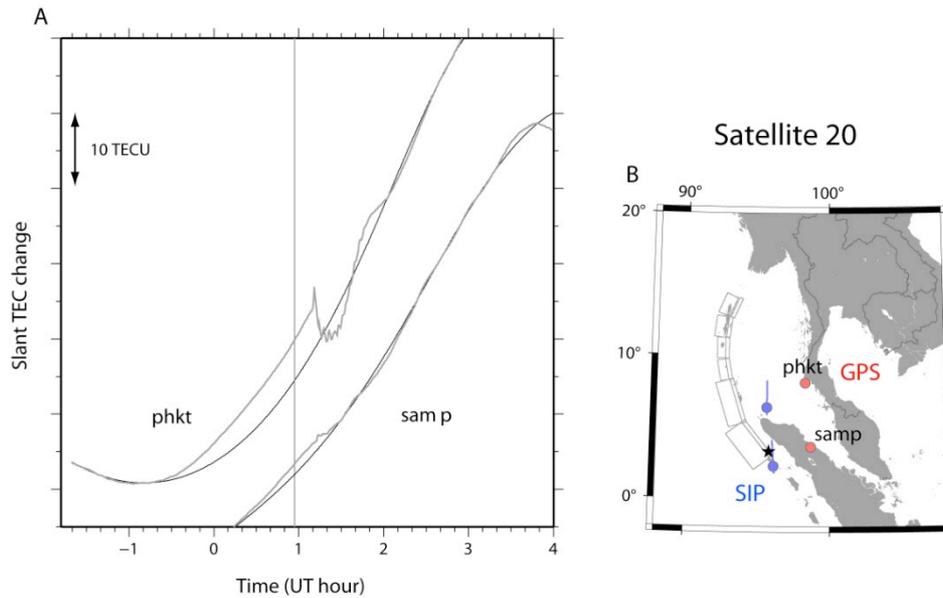
Figure S10. (**A**) Slant TEC change time series observed at two GPS stations in Indonesia (samp) and Thailand (phkt) with the satellite 20. Black smooth curves are the models derived assuming vertical TEC changing according to cubic polynomials of time (−0.5-1.2 UT is excluded in estimating the model curves). The 2004 December 26 Sumatra-Andaman earthquake occurred at 0:58 UT. Its fault planes [*Banerjee et al.*, 2005] are shown by rectangles in (**B**). Their 0.0-1.2 SIP trajectories (blue dots indicate 0:58) are plotted as blue curves. Preseismic electron increase seems to have started ~90 minutes before the earthquake.
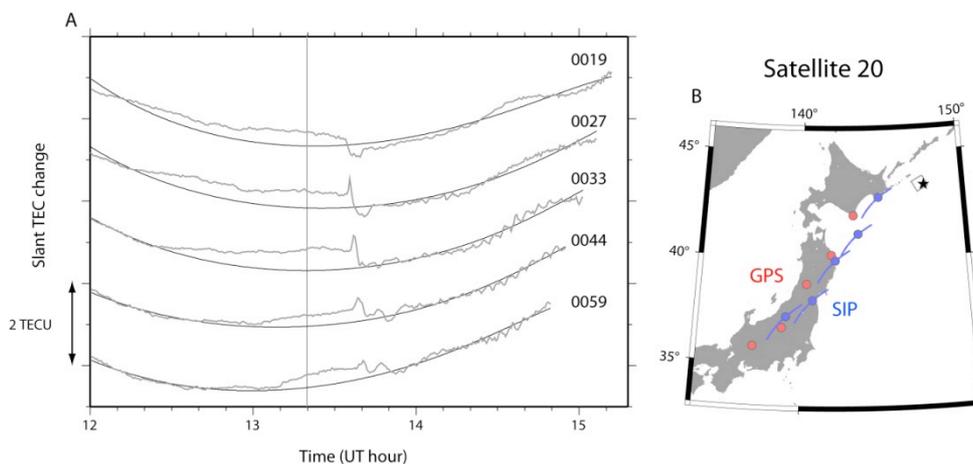
Figure S11. (**A**) Slant TEC change time series observed at five GPS stations in eastern Japan with the satellite 20. Black smooth curves are the models derived assuming vertical TEC changing according to cubic polynomials of time (12.5-13.8 UT is excluded in estimating the model curves). The 1994 October 4 Hokkaido-Toho-Oki earthquake occurred at 13:22 UT. Its fault plane [*Tsuji et al.*, 1995] is shown in (**B**). Their 12.5-13.8 SIP trajectories (blue dots

indicate 13:22) are plotted as blue curves. Preseismic electron increase seems to have started ~50 minutes before the earthquake. TEC increase is much smaller than the three M9 class earthquakes (Fig.4).
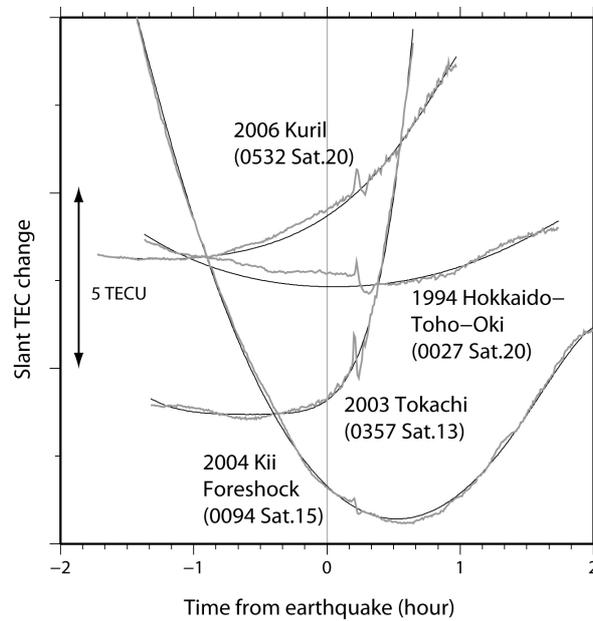
Figure S12. TEC behaviors within ±2 hours from the four M7-8 class earthquakes whose CIDs have been studied with GEONET [*Astafyeva and Heki*, 2009; *Heki and Ping*, 2005]. Their SIPs are located within 200 km from the epicenter, and CIDs appear ~10 minutes after the earthquakes. Weak TEC enhancements are seen before the 1994 ($M_w8.3$) and 2006 ($M_w8.2$) earthquakes, but not before the 2003 ($M_w8.0$) and 2004 ($M_w6.9$) earthquakes (Fig.4B).